sensors

MDPI

Article

Selective Detection of Nitrogen-Containing Compound Gases

Ran Yoo [1,†], Hyun-Sook Lee [1,†], Wonkyung Kim [2], Yunji Park [1], Aran Koo [1], Sang-Hyun Jin [3], Thang Viet Pham [4], Myung Jong Kim [4], Sunglyul Maeng [3,*] and Wooyoung Lee [1,*]

1 Department of Materials Science and Engineering, Yonsei University, 50 Yonsei-ro, Seodaemun-gu, Seoul 03722, Korea
2 School of Nano & Materials Science and Engineering, Kyungpook National University, 2559 Gyeongsang-daero, Gyeongsangbuk-do 37224, Korea
3 Isenlab Inc., Halla Sigma Valley, Dunchon-daero 545, Jungwon-gu, Seongnam-si, Gyeonggi-do 13215, Korea
4 Department of Electrical and Electronic Engineering, Woosuk University, 443, Samnye-ro, Samnye-eup, Wanju_Gun, Jeollabuk-do 55338, Korea
5 Functional Composite Materials Research Center and Division of Nano & Information Technology of KIST School, Korea Institute of Science and Technology, Jeonbuk 565-905, Korea
* Correspondence: sunglyulm@gmail.com (S.M.); wooyoung@yonsei.ac.kr (W.L.)
† These authors contributed equally.

Received: 4 July 2019; Accepted: 7 August 2019; Published: 15 August 2019

Abstract: N-containing gaseous compounds, such as trimethylamine (TMA), triethylamine (TEA), ammonia (NH_3), nitrogen monoxide (NO), and nitrogen dioxide (NO_2) exude irritating odors and are harmful to the human respiratory system at high concentrations. In this study, we investigated the sensing responses of five sensor materials—Al-doped ZnO (AZO) nanoparticles (NPs), Pt-loaded AZO NPs, a Pt-loaded WO_3 (Pt-WO_3) thin film, an Au-loaded WO_3 (Au-WO_3) thin film, and N-doped graphene—to the five aforementioned gases at a concentration of 10 parts per million (ppm). The ZnO- and WO_3-based materials exhibited n-type semiconducting behavior, and their responses to tertiary amines were significantly higher than those of nitric oxides. The N-doped graphene exhibited p-type semiconducting behavior and responded only to nitric oxides. The Au- and Pt-WO_3 thin films exhibited extremely high responses of approximately 100,000 for 10 ppm of triethylamine (TEA) and approximately −2700 for 10 ppm of NO_2, respectively. These sensing responses are superior to those of previously reported sensors based on semiconducting metal oxides. On the basis of the sensing response results, we drew radar plots, which indicated that selective pattern recognition could be achieved by using the five sensing materials together. Thus, we demonstrated the possibility to distinguish each type of gas by applying the patterns to recognition techniques.

Keywords: chemical sensors; nitrogen-containing compound gases; trimethylamine; triethylamine; ammonia; NO; NO_2; Al-doped ZnO nanoparticles; WO_3 thin film; N-doped graphene

1. Introduction

Many N-containing gases exude irritating odors, such as ammonia (NH_3), trimethylamine (TMA), triethylamine (TEA), nitric oxide (NO), and nitrogen dioxide (NO_2). NH_3 mainly arises from natural sources through the decomposition of organic matter containing nitrogen. Exposure to high levels of NH_3 emitted from chemical plants, cultivated farmland (fertilizer), and motor vehicles can cause irritation and serious burns on the skin and in the mouth, throat, lungs, and eyes [1,2].

TMA is a colorless, hygroscopic, and flammable tertiary amine that has a strong fishy odor at low concentrations and an NH_3-like odor at higher concentrations. Exposure to high levels of TMA can cause headaches, nausea, and irritation to the eyes and respiratory system. After marine fish death,

bacterial or enzymatic actions rapidly convert trimethylamine oxide into TMA—a volatile base that is largely responsible for the characteristic odor of dead fish [3,4]. Accordingly, the detection of TMA is essential for evaluating the freshness of fish [5–7]. TEA is a colorless volatile liquid with a strong fishy odor, reminiscent of the smells of NH_3 and the hawthorn plant [8]. It is commonly utilized as a catalyst and an acid neutralizer for condensation reactions, and is useful as an intermediate for manufacturing medicines, pesticides, and other chemicals. It is also a decomposition product of the V-series nerve gas agent [9]. Short-term exposure to TEA can irritate the skin and mucous membranes of humans. Chronic (long-term) exposure of workers to TEA vapor can cause reversible corneal edema [10].

NO is a nonflammable, extremely toxic, oxidizing gas with a sharp sweet odor. NO can be released by the reaction of nitric acid with metals, e.g., in metal etching and pickling, and is a byproduct of the combustion of substances in fossil fuel plants and automobiles. NO is a skin, eye, and mucous membrane irritant, as moisture and O_2 convert nitric oxide into nitric and nitrous acids. The most hazardous effects of NO are on the lungs. Inhalation causes symptoms such as coughing and shortness of breath, along with a burning sensation in the throat and chest [11]. NO is spontaneously converted to NO_2 in air; thus, some NO_2 is likely to be present when nitric oxide is detected in air [12]. NO_2 has a strong harsh odor, similar to chlorine, and may exhibit a vivid orange color. The major source of NO_2 is the burning of coal, oil, and gas. Almost all NO_2 comes from motor-vehicle exhaust, metal refining, electricity generation from coal-fired power plants, and other manufacturing industries [13]. The reaction of NO_2 with chemicals produced by sunlight leads to the formation of nitric acid, which is a major constituent of acid rain [14]. NO_2 also reacts with sunlight, which leads to the formation of ozone and smog in air [15,16]. The main effect of breathing high levels of NO_2 is an increased risk of respiratory problems, such as asthma, wheezing, coughing, colds, the flu, and bronchitis [17,18]. The U.S. National Institute for Occupational Safety and Health (NIOSH) has established exposure limits for these gases, as shown in Table 1 [19].

Various sensing materials have been investigated for the detection of N-containing compound gases. For the detection of tertiary amines (TMA, TEA), metal oxides, such as TiO_2, WO_3, MoO_3, $LaFeO_3$, SnO_2, and ZnO, have been tested [20–32]. Sensing materials based on WO_3, $MoSe_2$, multi-walled C nanotubes, and graphene oxide have been reported to exhibit good sensitivity to NH_3 gas [33–41]. Nitric oxide (NO, NO_2) sensing has recently been performed using metal oxides, such as ZnO, SnO_2, and WO_3, and metal–polymer composites, such as nickel phthalocyanine (NiPc) and graphene [42–53]. However, the highly sensitive and selective detection of N-containing compounds is urgently required.

In this study, we investigated the sensing properties of Al-doped ZnO (AZO) nanoparticles (NPs), Pt-loaded AZO (Pt-AZO) NPs, a Pt-loaded WO_3 (Pt-WO_3) thin film, a Au-loaded WO_3 (Au-WO_3) thin film, and N-doped graphene toward NH_3, TMA, TEA, NO, and NO_2. We found that each N-based hazardous gas reacted distinctively to the five types of sensing materials, producing different sensing patterns.

Table 1. Exposure limits for the gases established by the U.S. National Institute for Occupational Safety and Health.

Gas	Short-Term Exposure Limit (15 min, ppm)	Time Weighted Average (8 h, ppm)
NH_3	50	35
TMA	15	10
TEA	25	15
NO	-	25
NO_2	5	3

2. Materials and Methods

2.1. Synthesis

2.1.1. AZO NPs

AZO NPs were synthesized via a hydrothermal method [54,55]. Zinc acetate dehydrate ($Zn(AC)_2 \cdot 2H_2O$, 99%, Sigma-Aldrich, Seoul, Korea) and potassium hydroxide (KOH, 99%, Sigma-Aldrich) were dissolved in methanol with a molar ratio of 1:3. Aluminum acetate (99%, Sigma-Aldrich) was placed into the zinc acetate solution to achieve 1.0 at% of doped Al. The KOH solution was mixed with the zinc acetate solution via stirring at 60 °C for 24 h. Then, the suspension was centrifuged and washed with methanol three times. The obtained samples were dried at 90 °C for 60 min and annealed at 350 °C for 30 min in a H_2/N_2 atmosphere.

2.1.2. Pt-AZO NPs

For synthesizing Pt-AZO NPs, Pt NPs were coated on the surface of the as-synthesized AZO NPs with a deposition rate of 6−7 nm/min using a DC magnetron sputtering system in an agitated vessel [55]. In the agitated vessel, the powders were continuously stirred using a rotating impeller, and the Pt NPs were homogenously loaded on the surface of the AZO NPs. The Pt-loaded samples were prepared with a deposition time of 2 min.

2.1.3. Pt-WO_3 and Au-WO_3 Thin Films

For synthesizing Pt-WO_3 and Au-WO_3 thin films, WO_3 thin films were prepared via dual ion beam sputtering [56]. A tungsten metal target of 99.99% purity was employed. The WO_3 was deposited onto an interdigitated Pt electrode formed on a Si/SiO_2 wafer via a photolithography process. The dual ion beam consisted of a primary ion beam applied to the target and a secondary ion beam with accelerated atoms to be deposited on the substrate. The tungsten target was sputtered under the following conditions: The power of the main ion gun was 90 W, the voltage of the anode was 50 V, and the voltage of the cathode was −50 V. O ions were applied under the following conditions: The power of the assistant ion gun was 120 W, the voltage of the anode was 1000 V, and the voltage of the cathode was 300 V. The thickness of the WO_3 thin film was 200 nm. Pt (2 nm) and Au (2 nm) were deposited on the WO_3 thin film via direct current (DC) magnetron sputtering as catalysts. The thickness of Au and Pt was adjusted to ~2 nm by controlling the deposition time, where the deposition rate was 0.67 nm/s for Au and 0.28 nm/s for Pt. The samples were heat-treated at 550 °C for 1 h.

2.1.4. N-Doped Graphene

N-doped graphene was synthesized via arc discharging. A hollow graphite rod with a size of 6 mm, bismuth oxide as a catalyst, and 4-aminobenzoic acid as a dopant were placed into the hole and discharged while inducing 150 A in a 550 Torr H_2/He atmosphere used as a buffer. The amount of N in the graphene was 2 wt% [57].

2.1.5. Summary of Sensing Materials

Table 2 presents the fabrication methods and specifications for the five aforementioned sensing materials used in the experiments.

Table 2. Fabrication methods and specifications for the five sensing materials.

Sensing Materials	Fabrication Method	Specifications
AZO NPs	Hydrothermal synthesis	AZO NPs Size: 20–30 nm
Pt-AZO NPs	Hydrothermal synthesis + sputtering	AZO NPs size: 20–30 nm Pt NPs size: 2–3 nm Al doping: 1 at%
Pt-WO_3 thin film	Dual ion beam sputtering	WO_3 thickness: 200 nm Pt thickness: 2 nm
Au-WO_3 thin film	Dual ion beam sputtering	WO_3 thickness: 200 nm Au thickness: 2 nm
N-doped graphene	Arc discharge of graphite	N doping: 2 wt%

2.2. Characterization

The morphology and shape of the as-synthesized sensing materials were investigated via field-emission scanning electron microscopy (FE-SEM, JEOL 7001F) and transmission electron microscopy (TEM, JEOL JEM-ARM200F).

2.3. Device Fabrication

For fabrication of the gas sensor, interdigitated Cr (20 nm) and Pt (100 nm) electrodes were deposited on the patterned SiO_2 substrate via DC magnetron sputtering [54,55]. The synthesized NPs (AZO and Pt-AZO NPs) were mixed with an α-terpineol binder and coated onto the interdigitated electrodes. The sensor was heat-treated at 300 °C for 1 h to remove the binder and annealed at 600 °C for 1 h. The Pt-WO_3 and Au-WO_3 thin films were sputtered directly onto the interdigitated electrodes. N-doped graphene was drop-coated onto the electrodes.

2.4. Gas Sensing Measurement

A device was mounted in a chamber of a tube furnace system and placed in a flow system equipped with gas cylinders and mass flow controllers (MFCs) to perform the gas sensing test. The working temperature of the sensor was controlled using the temperature controller of the tube furnace. With the application of controlled heat, the resistance of the sensing material was measured in the presence of synthetic air and then in the presence of air with a controlled amount of target gas. The amount of target gas was controlled to 10 parts per million (ppm) by varying the gas flow rates using the MFCs. All the gas sensing measurements were conducted at an operating temperature of 400 °C, except for N-doped graphene (room temperature). The sensing properties were measured using a combination of a current source (Keithley 6220) and a nanovoltmeter (Keithley 2182) with a constant current supply of 10 nA.

3. Results and Discussion

Figure 1 shows the size and morphology of the sensing materials. Figure 1a presents a TEM image of AZO NPs, which were spherical and had a diameter of ~25 nm. The isolated AZO NP represented the single crystallinity of a hexagonal wurtzite structure of ZnO with a lattice spacing of ~0.28 nm, which was confirmed by high-resolution TEM analysis with the electron diffraction pattern [54]. Figure 1b shows a TEM image of the as-synthesized Pt-AZO NPs. This indicates that the Pt NPs with a size of ~2 nm were uniformly distributed on the surface of the AZO NPs, which was confirmed by analyses of the high-angle annular dark-field scanning transmission electron microscopy (HAADF-STEM) image and the energy dispersive X-ray spectroscope (EDS) line profile [54,55]. In addition, the XRD patterns of AZO and Pt-AZO NPs revealed the crystal structure of a hexagonal wurtzite phase without any secondary or impurity phases [55]. The diffraction peaks of the face centered cubic structure of the Pt crystals were observed for Pt-AZO NPs [55]. Figure 1c shows a TEM image of strip-shaped N-doped

graphene with a diameter of ~10 nm. The basal planes were discontinuous and distorted, and some parts were wavy and turbostratic, indicating the presence of defects, which may have facilitated gas diffusion. Cross-sectional SEM images of the Au-WO_3 and Pt-WO_3 thin films are shown in Figure 1d,e, respectively. The thickness of the WO_3 thin film was ~200 nm. The thicknesses of the Pt and Au activator layers deposited on the WO_3 thin film were estimated to be ~2 nm.

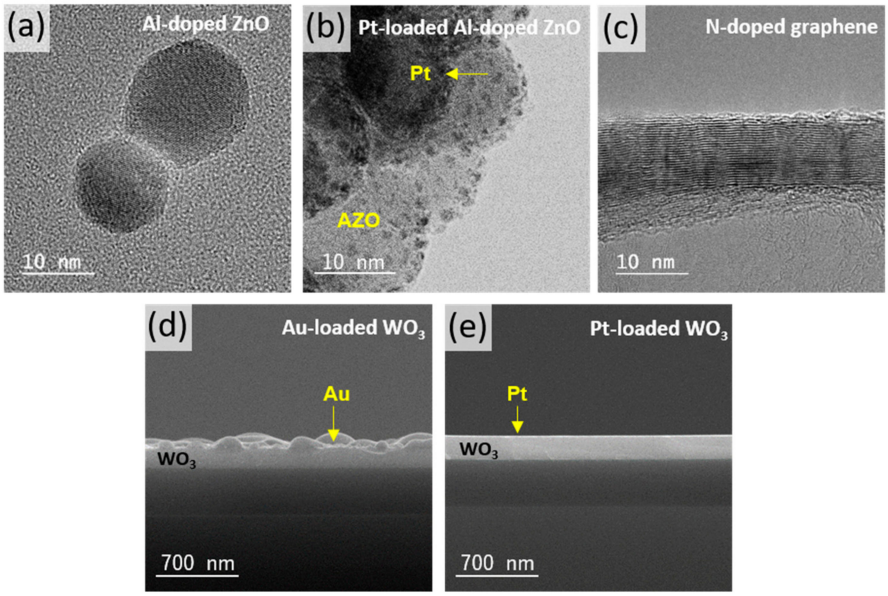

Figure 1. TEM images of (**a**) Al-doped ZnO (AZO) nanoparticles (NPs), (**b**) Pt-AZO NPs, and (**c**) N-doped graphene and SEM images of (**d**) the Au-loaded WO_3 (Au-WO_3) thin film and (**e**) the Pt-loaded WO_3 (Pt-WO_3) thin film.

Figure 2 shows the response patterns of the sensing materials exposed to 10 ppm of NO, NO_2, NH_3, TMA, and TEA gases. Here, the sensing response is defined as $(R_a - R_g)/R_g$, depending on whether the gas is reducing or oxidizing, where R_g and R_a represent the resistances of the five types of sensing materials in the N-containing compound gases and air, respectively. In this figure, the upward and downward directions of the graph correspond to the decrease and increase of the resistance, respectively. As shown in Figure 2, the responses of the metal oxides (AZO, Pt-AZO, Pt-WO_3, Au-WO_3) became positive when they were exposed to reducing gases (NH_3, TMA, TEA) and negative under exposure to oxidizing gases (NO, NO_2). This is because all the metal oxides tested in this experiment were n-type semiconductors. Positive and negative responses correspond to the decrease and increase, respectively, of the resistance of the sensing material in the target gas compared with that in air. In contrast, the responses of the N-doped graphene became positive when it was exposed to oxidizing gases (NO, NO_2), indicating that N-doped graphene is a p-type semiconductor.

Figures 3–5 show graphical representations of the sensing responses (in Figure 2) of the sensors to the N-containing compound gases. Figure 3a presents the sensing responses of AZO NPs to the five N-containing compound gases. The AZO NPs exhibited a decrease in resistance when exposed to 10 ppm TEA, TMA, and NH_3. Among these, the highest response level was 144 for TEA. The responses were 44 and 24 for TMA and NH_3, respectively (see Figure 2a). When the AZO NPs were exposed to 10 ppm NO and NO_2, an increase in resistance was observed, with response values of −0.06 and −0.07 in NO and NO_2, respectively.

Figure 3b presents the sensing responses of Pt-AZO NPs to the N-containing compound gases. The Pt-AZO NPs exhibited a higher overall response to the N-based hazardous gases than the AZO NPs (see Figure 2b). Additionally, the Pt-AZO NPs showed a reduced resistance when exposed to 10 ppm TEA, TMA, and NH_3, with response values of 159, 73, and 23, respectively. When exposed to NO and NO_2, the resistance increased, and the response was −2.8 and −4.7, respectively. Compared with pure

AZO, the Pt-ZNO NPs exhibited almost no change in their response to NH_3, whereas their response was increased slightly and significantly for the tertiary amines and nitric oxides, respectively. The sensing response of sensing materials can be augmented via noble-metal loading [58]. Consequently, in various gas sensing applications, Pt is loaded as a catalytic additive for enhancing the sensing response [55,59]. In our case, the Pt loading was effective for improving the nitric-oxide sensing.

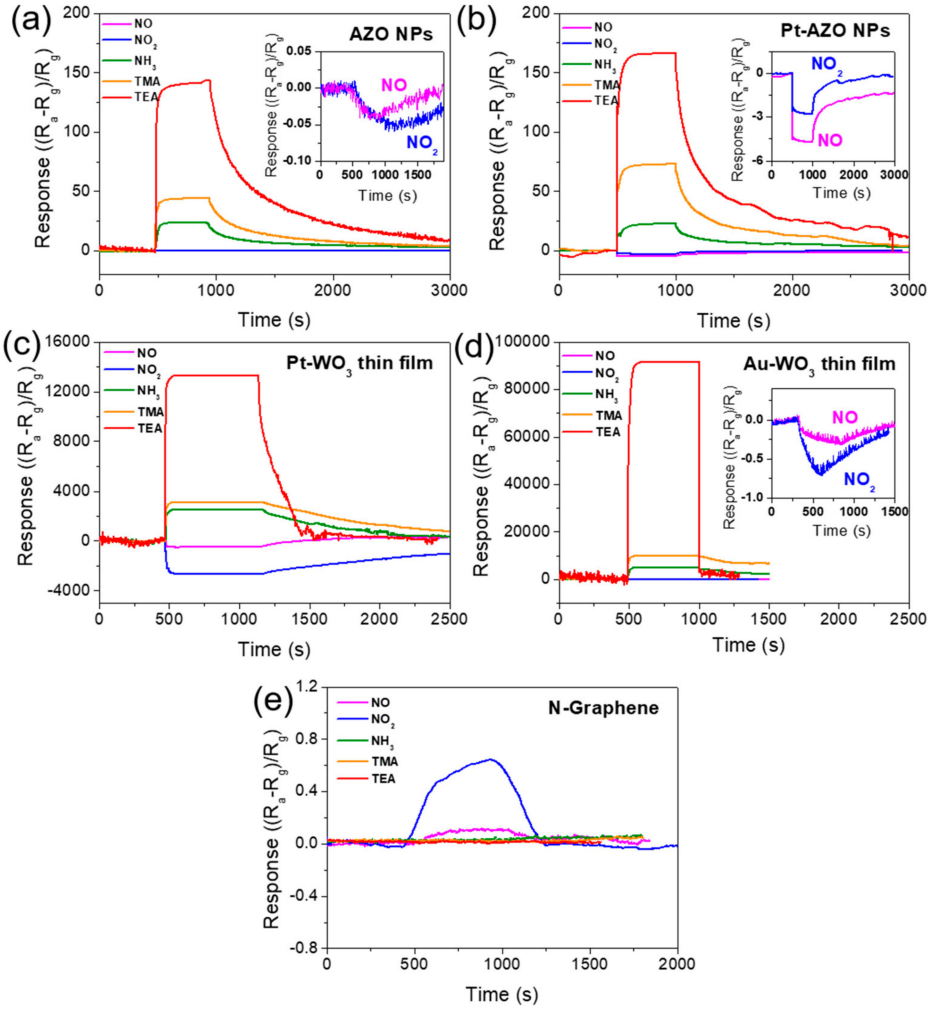

Figure 2. Variation in the sensing responses to 10 ppm of the five N-containing compound gases for the (**a**) AZO NPs, (**b**) Pt-AZO NPs, (**c**) Pt-WO_3 thin film, (**d**) Au-WO_3 thin film, and (**e**) N-doped graphene at 400 °C.

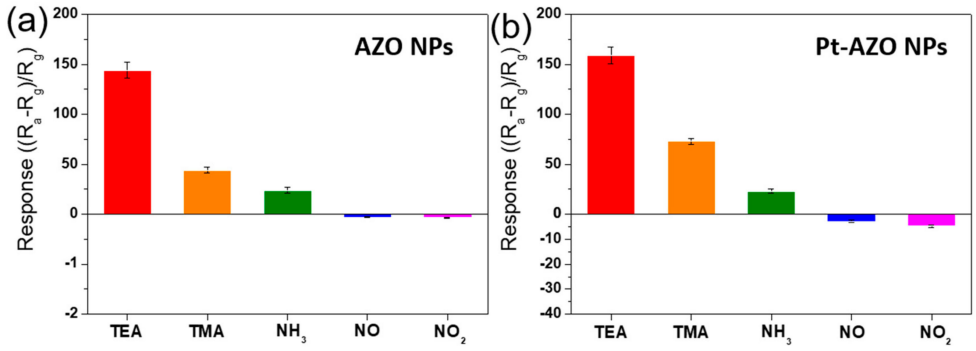

Figure 3. Bar graph of the sensing responses of the (**a**) AZO and (**b**) Pt-AZO NPs to 10 ppm of the N-containing compound gases at 400 °C.

Figure 4a presents the sensing responses of the Pt-WO_3 thin film to the N-containing compound gases. The Pt-WO_3 exhibited high sensitivity to not only tertiary amines but also nitric oxides. The sensing responses of the Pt-WO_3 thin film to TEA, TMA, and NH_3 were 13,277, 3100, and 2489, respectively. The sensing responses to NO and NO_2 were −481 and −2638, respectively, indicating an increased resistance. Remarkably, the TEA sensing response exceeded ~13,000. To our knowledge, all the responses of the Pt-WO_3 thin film to TEA, TMA, NH_3, NO, and NO_2 are significantly higher than those of previously reported sensing materials based on semiconducting metal oxides (See Table 3).

Figure 4b shows the sensing responses of the Au-WO_3 thin film to the N-containing compound gases. The sensing responses of the Au-WO_3 thin film to TEA, TMA, and NH_3 were 93,666, 9810, and 4821, respectively. The sensing responses of NO and NO_2 were −0.29 and −0.71, respectively. The Au-WO_3 thin film exhibited much higher response to TEA, TMA, and NH_3 than the Pt-WO_3 thin film. In particular, the Au-WO_3 thin film exhibited an extremely high sensing response (~100,000) to TEA compared to the other gases. To our knowledge, this is the first report of the highest sensing response to TEA, TMA, and NH_3, compared to those reported so far, for metal-oxide sensing materials (See Table 3).

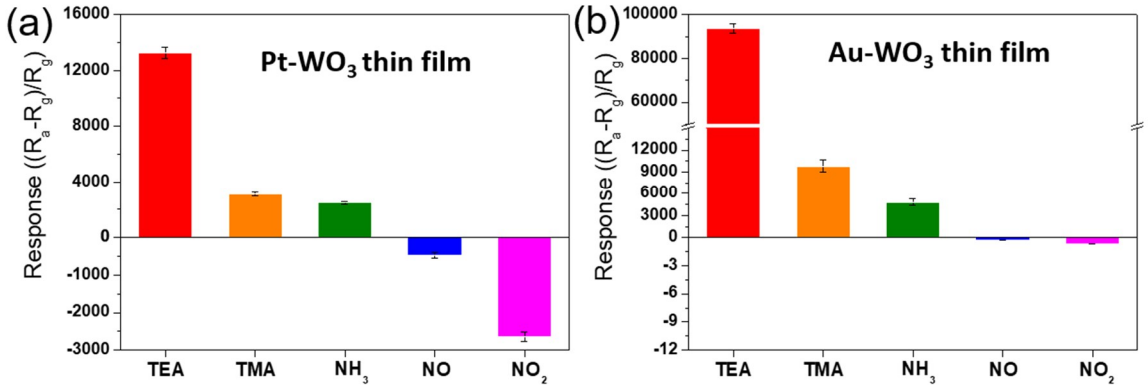

Figure 4. Bar graph of the sensing responses of the (**a**) Pt- and (**b**) Au-WO_3 thin films to 10 ppm of the N-containing compound gases at 400 °C.

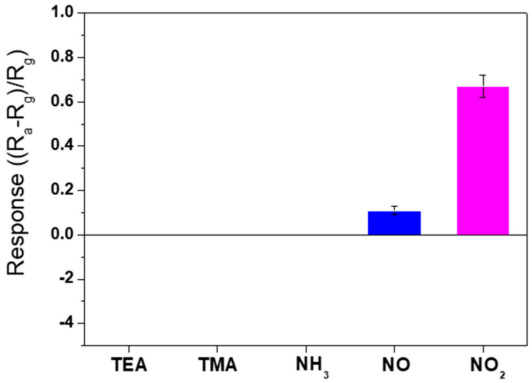

Figure 5. Bar graph of the sensing responses of the N-doped graphene to 10 ppm of the N-containing compound gases at 400 °C.

Figure 5 shows the sensing responses of N-doped graphene to the N-containing compound gases. NH_3 and the tertiary amines were not detected, even at a relatively high concentration (10 ppm); only nitric oxides were detected, with a low response of 0.1–0.7. Pure graphene is a p-type semiconductor in air, and exposure to oxidizing gases, such as NO_2 and O_2, reduces its resistance by enhancing the hole conduction [60]. Although Lu et al. reported that highly N-doped graphene exhibits n-type semiconducting behavior [61], the sensing response of our N-doped graphene indicated that the sample was a p-type semiconductor. If the doped N atoms replace the C atoms in the hexagonal ring of

graphene (quaternary N) efficiently, 2 wt% N in graphene is sufficient to make the material an n-type semiconductor. Thus, our results indicate that the direct substitutional doping was not efficient enough to make the material n-type. When N atoms are doped into graphene, three bonding configurations occur within the C lattice: Quaternary N (direct substitution), pyridinic N, and pyrrolic N [57]. Only quaternary N yields n-type doping; the other two configurations promote p-type doping [62].

The XPS N 1s spectra of the N-doped graphene used in our experiments presented that the amount of pyridinic and pyrrolic N was larger than that of quaternary N [57]. As shown in Figure 5, the N-doped graphene exhibited good sensitivity to NO_2. This was expected, as Shaik et al. reported NO_2 sensing with N-doped graphene, which was fabricated using a wet process and exhibited p-type behavior [63]. In contrast, the theoretical studies of Jappor et al. and Dai et al. [64,65], which focused on quaternary N-doping, indicated that NO_2 was weakly physiosorbed onto the N-doped graphene surface. Clearly, the pyridinic and pyrrolic N-doping made graphene a good NO_2 gas sensor.

Figure 6 shows the response of AZO NPs, Pt-AZO NPs, Au-WO_3 thin film, and Pt-WO_3 thin film at various concentrations of the five N-containing gases (0.1, 1, and 10 ppm) at 400 °C. The sensing response increases with increasing gas concentration. As shown in Figure 6, the ZnO and WO_3 samples have a lower limit of 0.01 ppm to detect those N-containing gases.

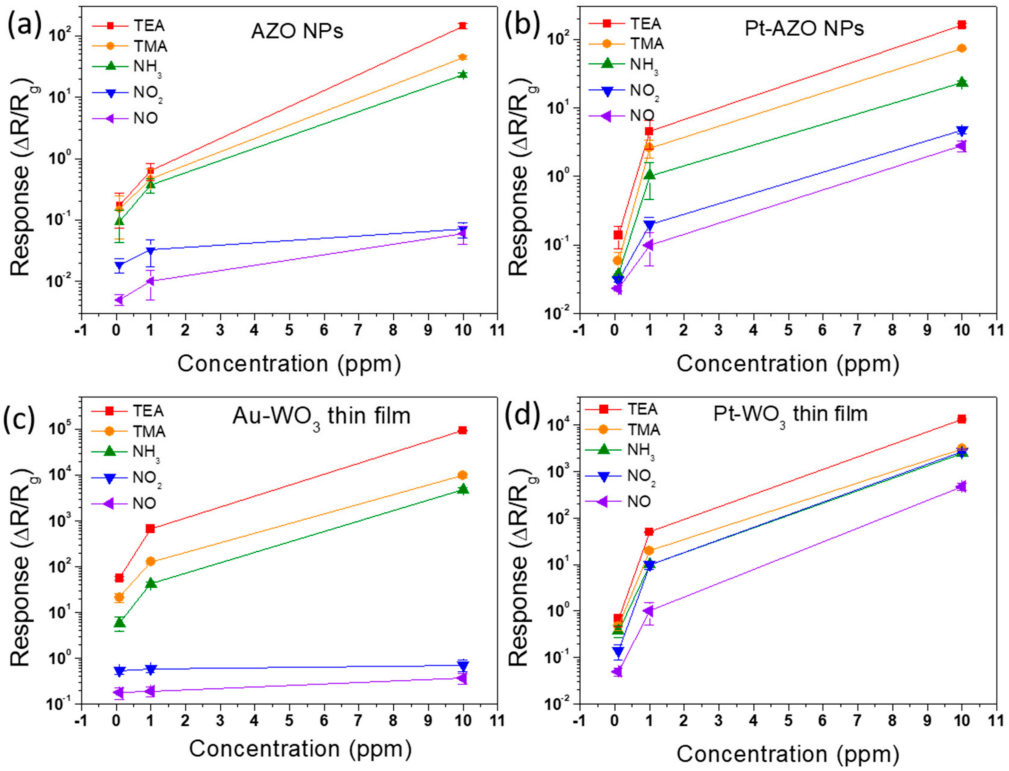

Figure 6. Sensing response of (**a**) AZO NPs, (**b**) Pt-AZO NPs, (**c**) Au-WO_3 thin film, and (**d**) Pt-WO_3 thin film to different concentrations of the five N-containing gases at 400 °C.

A comparison of the responses of the five sensing materials to 10 ppm of the five N-containing compound gases is shown in Figure 7a–e in the form of radar plots. The radar plots of the sensing response show different patterns for the reducing gases (TEA, TMA, NH_3) and the oxidizing gases (NO, NO_2). The specific patterns of the radar plots for the sensing response represent several noteworthy features: (i) The sensing response of the WO_3 film-based sensor was superior to that of the AZO NP-based sensor for all five N-containing compound gases; (ii) the WO_3 film and AZO NP-based sensors are more sensitive in detecting TEA compared to the other gases; (iii) the Au-WO_3 thin film exhibited the highest response for the detection of 10 ppm of TEA, TMA, and NH_3; (iv) the Pt-WO_3 thin film showed the best sensing performance for the detection of 10 ppm of NO and NO_2.

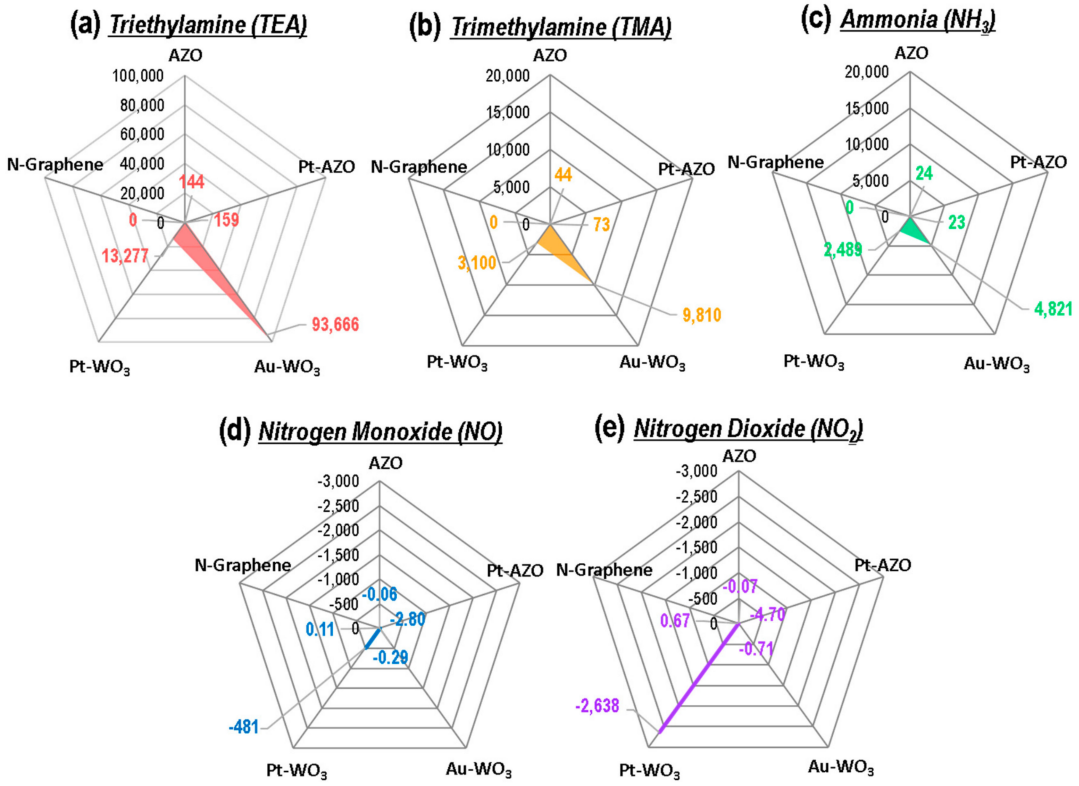

Figure 7. Radar plots of the sensing responses $((R_a - R_g)/R_g)$ of the five sensing materials to 10 ppm of (**a**) TEA, (**b**) TMA, (**c**) NH_3, (**d**) NO, and (**e**) NO_2.

In particular, the sensing response of the WO_3 film and AZO NP-based sensors increases in the order of NH_3, TMA, and TEA. The response is significantly higher in detecting TEA compared to the other gases. This can be attributed to an electron donating effect [25]. When the metal oxide sensor is exposed to the reducing gas, the reducing gas reacts with the adsorbed oxygen ions and the free electrons are released back to the conduction band of the metal oxides. This leads to an increase in conductance and consequently an increase in response. At the working temperature of WO_3 film and AZO NP (400 °C), the O^{2-} ion species mainly interact with the gas molecules [55], according to the following equations for TEA (Equation (1) [24]), TMA (Equation (2) [28]), and NH_3 (Equation (3) [38]):

$$2(C_2H_5)_3N_{(ads)} + 43O_{(ads)}{}^{2-} \rightarrow 12CO_{2(gas)} + 15H_2O_{(gas)} + 2NO_{2(gas)} + 86e^- \quad (1)$$

$$2(CH_3)_3N_{(ads)} + 21O_{(ads)}{}^{2-} \rightarrow 6CO_{2(gas)} + 9H_2O_{(gas)} + N_{2(gas)} + 42e^- \quad (2)$$

$$2NH_{3(ads)} + 3O_{(ads)}{}^{2-} \rightarrow 9H_2O_{(gas)} + N_{2(gas)} + 6e^- . \quad (3)$$

As a consequence, a number of the released electrons increases in the order of NH_3, TMA, and TEA. Therefore, the significantly enhanced sensing response to TEA is mainly attributed to the great number of released electrons.

In addition, the responses of the Au-WO_3 thin film for sensing TEA, TMA, and NH_3 are remarkably better than those of the Pt-WO_3 thin film. To understand this result, we investigated the surface morphology and compositional distribution of those WO_3 thin films by using FE-SEM equipped with an energy-dispersive X-ray spectroscope (EDS). Figure 8 shows the top-view SEM images of the as-prepared Pt- and Au-WO_3 thin films. The images show the Pt particles cover the surface of the WO_3 thin film (Figure 8a), while the Au islands are randomly distributed on its surface (Figure 8b).

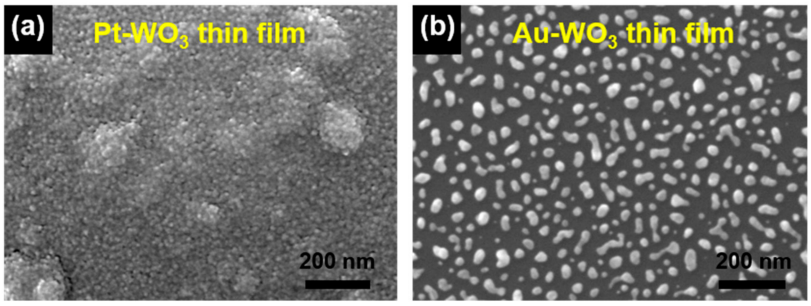

Figure 8. Top-view SEM images of the (**a**) Pt- and (**b**) Au-WO_3 thin films.

Figures 9 and 10 show the elemental distribution at the cross-sectional areas of the Pt- and Au-WO_3 thin films, respectively. The EDS elemental color mapping results present that the Pt elements cover the entire surface of the film, but the Au elements are sparsely distributed compared to Pt. According to the sensing mechanism, the sensing response of the n-type metal oxide gas sensor mainly depends upon the concentration of oxygen ion species (O^- or O^{2-}) adsorbed on the surface of the sensing materials. Further, the loaded noble metals provide more active sites for the adsorption of oxygen ion species owing to a spill-over effect. Therefore, too many Pt atoms covered on the film decreases the number of active sites available on the film's surface, leading to the reduced response. Consequently, the Au-WO_3 thin film exhibits better sensing response compared to the Pt-WO_3 thin film for the reducing gases of TEA, TMA, and NH_3. As a result, we can find that a moderate amount of metal catalyst plays an important role in improving the sensing response.

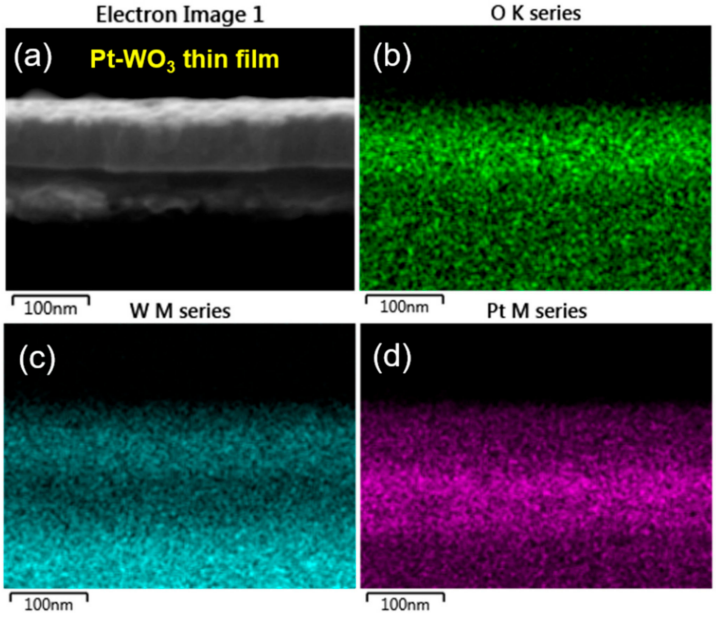

Figure 9. (**a**) Cross-sectional SEM image depicting analyzed region of Pt-WO_3 thin film and energy-dispersive X-ray spectroscope (EDS) elemental color mapping images for (**b**) O, (**c**) W, and (**d**) Pt elements.

More importantly, these sensing responses of the Au-WO_3 thin film to TEA, TMA, and NH_3, and the Pt-WO_3 thin film to NO and NO_2 are much higher than those of previously reported sensors based on metal-oxide sensing materials (See Table 3). The sensitivities of most metal-oxide sensors reported for the detection of TEA are very low. In addition, there are few reports on TEA detection using WO_3 materials. For example, polyaniline-WO_3 nanocomposites exhibited a sensing response of 81 to 100 ppm TEA at room temperature [23]. In the case of TMA sensing, there are many reports

showing good response results. Cho et al. reported a high response to 5 ppm TMA: 56.9 at 450 °C for a WO_3 hollow sphere [29] and 373.74 at 300 °C for MoO_3 nanoplates [30]. Sensing N-containing compound gases, such as NH_3 and NO_x, using Pt-WO_3 and Au-WO_3 has been reported. For example, D'Arienzo et al. reported that the sensing response of Pt-WO_3 to 74 ppm NH_3 was 110 at 225 °C [34]. Srivastava and Jain found that the sensing response of Pt-WO_3 to 4000 ppm NH_3 was 12 at 450 °C [35]. Maekawa et al. reported that Au-WO_3 (0.8–1.0 wt% Au) exhibited a good sensing response (40–60) to 50 ppm NH_3 gas at 450 °C [36]. For NO and NO_2 gas sensing, Penza et al. reported Au-WO_3 sensing responses of −100.3 (440 ppm) and −6.5 (10 ppm), respectively, at 150 °C [43]. Xia et al. reported that Au-WO_3 (1 wt% Au) exhibited a high sensing response (approximately −400) to 10 ppm NO_2 gas at 150 °C [48].

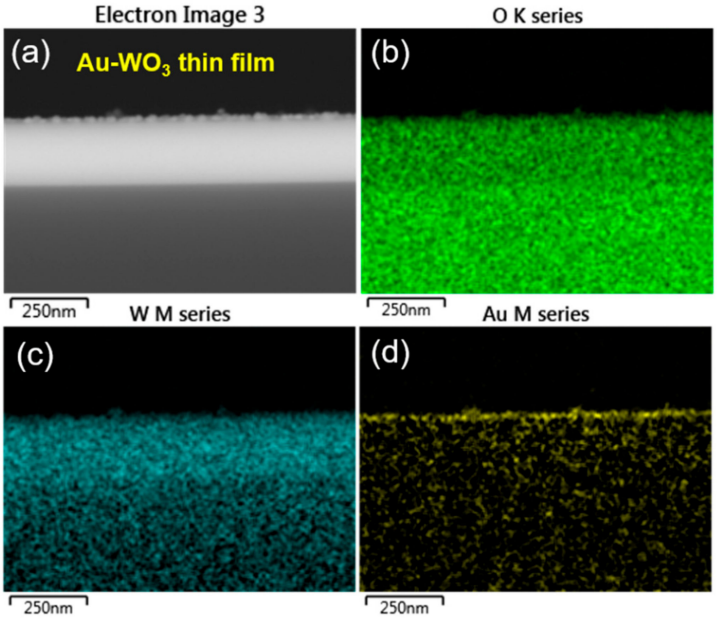

Figure 10. (**a**) Cross-sectional SEM image depicting analyzed region of Au-WO_3 thin film and EDS elemental color mapping images for (**b**) O, (**c**) W, and (**d**) Au elements.

Additionally, we evaluated the sensing responses of the five sensing materials to 10 ppm of the five N-containing compound gases, as presented in the form of the radar plots in Figure 11. The response time is defined as the time required to reach 90% of the saturation resistance upon the exposure to full-scale concentration of the gas. As shown in Figure 11, the Pt-WO_3 and Au-WO_3 thin films exhibited a fast response time (i.e., a very rapid reaction rate) for the detection of TEA, TMA, and NH_3. In particular, the Pt-WO_3 thin film showed high responses to all the N-containing gases, as well as the fastest response (<20 s).

The higher and faster sensing response of the Pt-WO_3 and Au-WO_3 thin films is attributed to the addition of an appropriate amount of metal additives to WO_3, which promoted chemical reactions by reducing the activation energy between the film surface and the target gas. Cu-loaded WO_3 and Ag-loaded WO_3 have also been reported to detect N-containing compound gases with high sensitivity [27,42]. Furthermore, the outstanding sensing responses of the Pt-WO_3 and Au-WO_3 thin films are attributed to the deposition of high-quality thin films via the dual ion beam sputtering technique. The thin films deposited using this technique exhibited an exact stoichiometry. Therefore, the dense thin-film formation allowed the deposition of high-quality films with a very small thickness. Furthermore, the five plot patterns are significantly different, indicating that the five sensor materials can be used for an e-nose to distinguish the five N-containing compound gases.

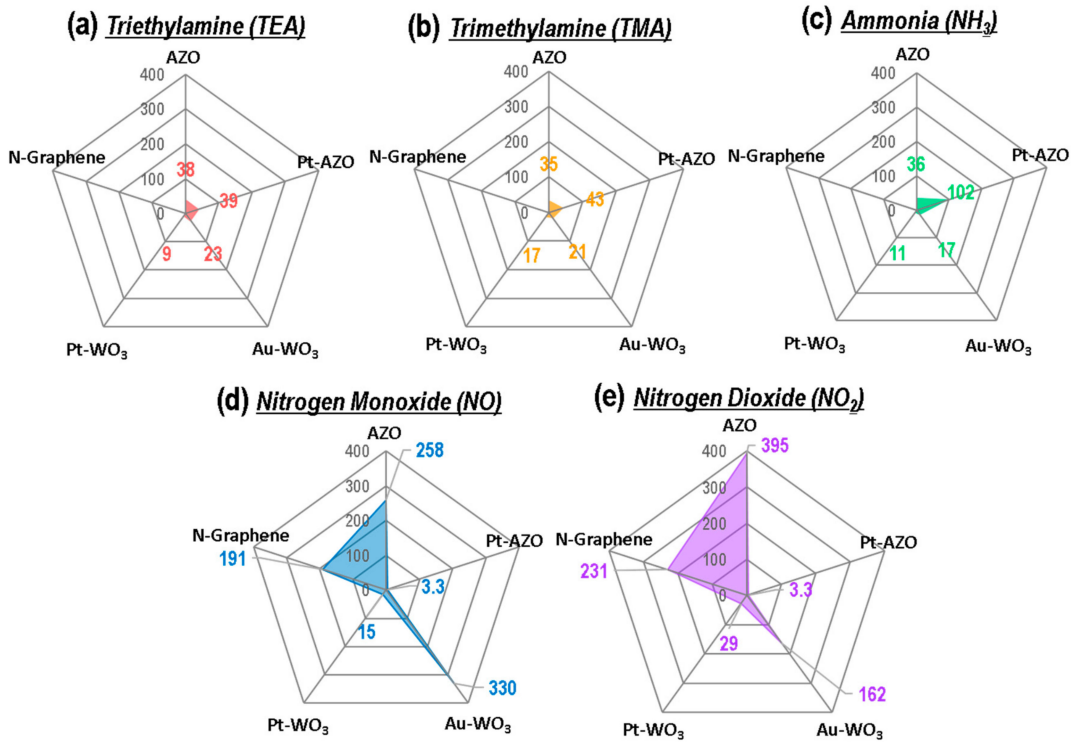

Figure 11. Radar plots of the response time (unit: sec) of the five sensing materials to 10 ppm of (**a**) TEA, (**b**) TMA, (**c**) NH_3, (**d**) NO, and (**e**) NO_2.

Table 3. Comparison of sensing properties of various types of metal-oxide-based sensors for the detection of the N-containing gaseous compounds ($\Delta R \equiv (R_a - R_g)$ or $(R_g - R_a)$, S *: Sensitivity ≡ response/concentration.).

Gas	Sensing Materials	Operating Temperature [°C]	Concentration [ppm]	Response (R/R_g)	S * [ppm^{-1}]	Ref.
TEA	Hollow SnO_2 microfiber	270	100	49.5	0.49	[20]
	ZnO-NiO hetero-nanostructures	250	200	35	0.17	[21]
	Au-Loaded ZnO/SnO_2 Core-Shell Nanorods	40	50	12.4	0.25	[22]
	polyaniline-WO_3 nanocomposites	25	100	80	0.8	[23]
	broken In2O3 microtubes	300	100	72.5	0.72	[24]
	CeO_2-SnO_2 Nanoflowers	310	200	252.2	1.26	[25]
	Al-doped ZnO (AZO) nanoparticles	400	10	144	14.4	This work
	Pt-loaded AZO nanoparticles	400	10	159	15.9	This work
	Au-loaded WO_3 thin film	400	10	93,666	9366.6	This work
	Pt-loaded WO_3 thin film	400	10	13,277	1327.7	This work

Table 3. *Cont.*

Gas	Sensing Materials	Operating Temperature [°C]	Concentration [ppm]	Response (R/R_g)	S * [ppm^{-1}]	Ref.
TMA	TiO_2	60	400	1.5	0.004	[26]
	membrane nanotubes	290	10	50	5	[27]
	Cu-doped WO_3 materials	325	5	120	24	[28]
	MoO_3 nanopapers	450	5	56.9	11.38	[29]
	WO_3 hollow spheres	300	5	374.74	74.95	[30]
	MoO_3 nanoplates	330	50	125	2.5	[31]
	SnO_2-ZnO nanocomposite	208	1000	2552	2.55	[32]
	Al-doped ZnO (AZO) nanoparticles	400	10	44	4.4	This work
	Pt-loaded AZO nanoparticles	400	10	73	7.3	This work
	Au-loaded WO_3 thin film	400	10	9810	981.0	This work
	Pt-loaded WO_3 thin film	400	10	3100	310.0	This work
NH_3	WO_3 Nanoparticles Thinfilm	240	0.5	2.3	4.6	[33]
	Macroporous WO_3 Thin Films	225	74	110	1.48	[34]
	Pt catalyzed WO_3 thick films	450	4000	15.5	0.004	[35]
	Au-loaded WO_3 powder	450	50	39	0.78	[36]
	single-layer $MoSe_2$ nanosheet	25	500	1150	2.3	[37]
	SnO Nanoshell	25	200	37.57	0.19	[38]
	SnO_2 nanostructures	300	800	222	0.28	[39]
	Al-doped ZnO (AZO) nanoparticles	400	10	24	2.4	This work
	Pt-loaded AZO nanoparticles	400	10	23	2.3	This work
	Au-loaded WO_3 thin film	400	10	4821	482.1	This work
	Pt-loaded WO_3 thin film	400	10	2489	248.9	This work
NO	Ag doped WO_3	250	40	38.3	0.96	[42]
	Pd doped WO_3	200	440	100.3	0.23	[43]
	Cu2+/Polyaniline/WO_3	25	0.04	9.6	240	[44]
	Al-doped ZnO (AZO) nanoparticles	400	10	0.06	0.006	This work
	Pt-loaded AZO nanoparticles	400	10	2.8	0.28	This work
	Au-loaded WO_3 thin film	400	10	0.29	0.03	This work
	Pt-loaded WO_3 thin film	400	10	481	48.1	This work
	N-doped graphene	400	10	0.11	0.01	This work

Table 3. *Cont.*

Gas	Sensing Materials	Operating Temperature [°C]	Concentration [ppm]	Response (R/R_g)	S * [ppm^{-1}]	Ref.
NO_2	WO_3 thin fim	200	0.01	28	2800	[46]
	plasma-sprayed WO_3 coating	130	0.45	77	171.1	[47]
	Pd doped WO_3	200	10	6.51	0.65	[43]
	Au-doped WO_3 powder	150	10	412	41.2	[48]
	ZnO hierarchical nanostructure	25	20	11.06	0.55	[50]
	SnO_2 nanoslab	300	10	120	12	[51]
	Al-doped ZnO (AZO) nanoparticles	400	10	0.07	0.007	This work
	Pt-loaded AZO nanoparticles	400	10	4.7	0.47	This work
	Au-loaded WO_3 thin film	400	10	0.71	0.07	This work
	Pt-loaded WO_3 thin film	400	10	2638	263.8	This work
	N-doped graphene	400	10	0.67	0.07	This work

4. Conclusions

We investigated the sensing properties of five types of sensing materials (AZO NPs, Pt-AZO NPs, a Pt-WO_3 thin film, a Au-WO3 thin film, and N-doped graphene) for the detection of five hazardous N-containing compound gases (TEA, TMA, NH_3, NO, and NO_2). Owing to the different reactivities of the gases, the sensing materials exhibited different sensing response patterns. The metal-oxide sensors of AZO, Pt-AZO, Pt-WO_3, and Au-WO_3 showed positive responses to NH_3, TMA, and TEA (reducing gases) and negative responses to NO and NO_2 (oxidizing gases). This is because all the metal oxides tested in the experiment were n-type semiconductors. In contrast, the N-doped graphene exhibited a positive response to NO and NO_2 owing to its p-type semiconducting property. The metal oxide-based materials showed significantly higher sensing responses to the tertiary amines than to the nitric oxides. The N-doped graphene reacted only to the nitric oxides. Among the sensing materials, the Au-WO_3 and Pt-WO_3 thin films exhibited the best sensing response. More importantly, the sensing responses of the Au-WO_3 thin film to TEA, TMA, and NH_3 and the Pt-WO_3 thin film to NO and NO_2 were much higher than those of previously reported sensors based on metal-oxide sensing materials. In particular, the Au-WO_3 and Pt-WO_3 thin films exhibited extremely high sensing responses of approximately 100,000 for 10 ppm of TEA and approximately −2700 for 10 ppm of NO_2, respectively. Accordingly, our study indicates that the five N-containing compound gases can be distinctively detected using the five sensor elements via application of recognition technology that shows different patterns of the sensing response. In order to demonstrate the analytical applicability of the proposed method in a real application, future studies will be conducted to investigate whether the sensor array consisting of the five sensing materials selectively detects only one target gas when mixed with the five N-containing compound gases. In addition, the reproducibility, long-term stability, and humidity interference of the sensor array will be tested.

Author Contributions: S.M. and W.L. conceived and designed the present study; R.Y. measured and analyzed the microscopic data and sensing data for all samples and wrote the paper; H.-S.L. analyzed all data and organized and wrote the paper; W.K., Y.P., and A.K. performed the synthesis of the ZnO-based nanoparticles and the WO_3-based thin films; S.-H.J. performed the synthesis of the N-doped graphene; and T.V.P. and M.J.K. contributed to the XPS measurement and analysis. All authors discussed the results and the implications of this manuscript.

Funding: This research was supported by the Priority Research Centers Program through the NRF (2019R1A6A1A11055660) and the Medium and Large Complex Technology Commercialization Project through the Commercialization Promotion Agency for R&D Outcomes (2019K000045). Both were funded by the Ministry of Science, ICT, and Future Planning.

Conflicts of Interest: The authors declare no conflict of interest.

References

1. Timmer, B.; Olthuis, W.; van den Berg, A. Ammonia sensors and their applications—A review. *Sens. Actuators B Chem.* **2005**, *107*, 666–677. [CrossRef]
2. Lippmann, M.; Schlesinger, R.B. *Chemical Contamination in the Human Environment*; Oxford University Press: New York, NY, USA, 1979.
3. Ringo, E.; Stenberg, E.; Stroem, A.R. Amino acid and lactate catabolism in trimethylamine oxide respiration of Alteromonas putrefaciens NCMS 1735. *Appl. Environ. Microbiol.* **1984**, *47*, 1084–1089. [PubMed]
4. Sadok, S.; Uglow, R.F.; Haswell, S.J. Determination of trimethylamine in fish by flow injection analysis. *Anal. Chim. Acta* **1996**, *321*, 69–74. [CrossRef]
5. Egashira, M.; Shimizu, Y.; Takao, Y. Trimethylamine sensor based semiconductive metal oxides for detection of fish freshness. *Sens. Actuators B Chem.* **1990**, *1*, 108–112. [CrossRef]
6. Moula, G.; Bose, M.; Sarkar, S. Replica of a fishy enzyme: Structure—Function analogue of trimethylamine-N-oxide reductase. *Inorg. Chem.* **2013**, *52*, 5316–5317. [CrossRef] [PubMed]
7. Wei, P.H.; Li, G.B.; Zhao, S.Y.; Chen, L.R. Gas-sensing properties of Th/SnO_2 thin film gas sensor to trimethylamine. *J. Electrochem. Soc.* **1999**, *146*, 3536–3537. [CrossRef]
8. Triethylamine, Wikimedia Foundation Inc. Available online: https://en.wikipedia.org/wiki/Triethylamine#cite_note-7 (accessed on 9 August 2019).
9. Perkins, F.K.; Friedman, A.L.; Cobas, E.; Campbell, P.M.; Jernigan, G.G.; Jonker, B.T. Chemical vapor sensing with monolayer MoS2. *Nano Lett.* **2013**, *13*, 668–673. [CrossRef]
10. Fonger, G.C. Hazardous Substances Data Bank (HSDB) as a source of environmental fate information on chemicals. *Toxicology* **1995**, *103*, 137–145. [CrossRef]
11. Your Best Option for Treating any Condition. Available online: http://www.kansashealthsystem.com/~{}/media/Imported/kumed/documents/nitricoxide.ashx?la=en (accessed on 9 August 2019).
12. Nitric Oxide Gas Detectors (NO Detectors). Available online: http://www.indsci.com/products/nitric-oxide/ (accessed on 9 August 2019).
13. Shi, Y.; Xia, Y.F.; Lu, B.H.; Liu, N.; Zhang, L.; Li, S.J.; Li, W. Emission inventory and trends of NOx for China, 2000–2020. *J. Zhejiang Univ. Sci. A* **2014**, *15*, 454–464. [CrossRef]
14. Atkinson, R. Atmospheric chemistry of VOCs and NOx. *Atmos. Environ.* **2000**, *34*, 2063–2101. [CrossRef]
15. Wilkins, C.K.; Clausen, P.A.; Wolkoff, P.; Larsen, S.T.; Hammer, M.; Larsen, K.; Hansen, V.; Nielsen, G.D. Formation of strong airway irritants in mixtures of isoprene/ozone and isoprene/ozone/nitrogen dioxide. *Environ. Health Perspect.* **2001**, *109*, 937–941. [CrossRef] [PubMed]
16. Nitrogen Oxides (Nitric Oxide, Nitrogen Dioxide, etc.). Available online: https://www.atsdr.cdc.gov/toxfaqs/tfacts175.pdf (accessed on 9 August 2019).
17. Nitrogen Dioxide (NO2). Available online: http://www.environment.gov.au/protection/publications/factsheet-nitrogen-dioxide-no2 (accessed on 9 August 2019).
18. Fahrländer, C.B.; Liebrich, U.A.; Schwartz, J.; Gnehm, H.P.; Rutishauser, M.; Wanner, H.U. Air pollution and respiratory symptoms in preschool children. *Am. Rev. Respir. Dis.* **1992**, *145*, 42–47. [CrossRef] [PubMed]
19. Index of Chemical Names. *1988 OSHA PEL Project Documentation*; The National Institute for Occupational Safety and Health (NIOSH): Cincinnati, OH, USA, 1988.
20. Zou, Y.; Chen, S.; Sun, J.; Liu, J.; Che, Y.; Liu, X.; Zhang, J.; Yang, D. Highly efficient gas sensor using a hollow SnO_2 microfiber for triethylamine detection. *ACS Sens.* **2017**, *2*, 897–902. [CrossRef] [PubMed]
21. Guo, T.; Luo, Y.; Zhang, Y.; Lin, Y.H.; Nan, C.W. ZnO-NiO hetero-nanostructures as highly sensitive and selective triethylamine sensor. *J. Appl. Phys.* **2014**, *116*, 044309. [CrossRef]
22. Ju, D.X.; Xu, H.Y.; Qiu, Z.W.; Zhang, Z.C.; Xu, Q.; Zhang, J.; Wang, J.Q.; Cao, B.Q. Near room temperature, fast-response, and highly sensitive triethylamine sensor assembled with Au-Loaded ZnO/SnO_2 core–shell nanorods on flat alumina substrates. *ACS Appl. Mater. Interfaces* **2015**, *7*, 19163–19171. [CrossRef]
23. Bai, S.; Ma, Y.; Luo, R.; Chen, A.; Li, D. Room temperature triethylamine sensing properties of polyaniline–WO_3 nanocomposites with p–n heterojunctions. *RSC Adv.* **2016**, *6*, 2687–2694. [CrossRef]

24. Yang, W.; Feng, L.; He, S.; Liu, L.; Liu, S. Density gradient strategy for preparation of broken In_2O_3 microtubes with remarkably selective detection of triethylamine vapor. *ACS Appl. Mater. Interfaces* **2018**, *10*, 27131–27140. [CrossRef]
25. Xue, D.; Wang, Y.; Cao, J.; Zhang, Z. Hydrothermal Synthesis of CeO2-SnO2 Nanoflowers for Improving Triethylamine Gas Sensing Property. *Nanomaterials* **2018**, *8*, 1025. [CrossRef]
26. Perillo, P.M.; Rodríguez, D.F. Low temperature trimethylamine flexible gas sensor based on TiO_2 membrane nanotubes. *J. Alloys Compd.* **2016**, *657*, 765–769. [CrossRef]
27. Zhu, S.; Liu, X.; Chen, Z.; Liu, C.; Feng, C.; Gu, J.; Liu, Q.; Zhang, D. Synthesis of Cu-doped WO_3 materials with photonic structures for high performance sensors. *J. Mater. Chem.* **2010**, *20*, 9126–9132. [CrossRef]
28. Li, H.Y.; Huang, L.; Wang, X.X.; Lee, C.S.; Yoon, J.W.; Zhou, J.; Guo, X.; Lee, J.H. Molybdenum trioxide nanopaper as a dual gas sensor for detecting trimethylamine and hydrogen sulfide. *RSC Adv.* **2017**, *7*, 3680–3685. [CrossRef]
29. Cho, Y.H.; Kang, Y.C.; Lee, J.H. Highly selective and sensitive detection of trimethylamine using WO_3 hollow spheres prepared by ultrasonic spray pyrolysis. *Sens. Actuators B Chem.* **2013**, *176*, 971–977. [CrossRef]
30. Cho, Y.H.; Ko, Y.N.; Kang, Y.C.; Kim, I.; Lee, J. Ultraselective and ultrasensitive detection of trimethylamine using MoO_3 nanoplates prepared by ultrasonic spray pyrolysis. *Sens. Actuators B Chem.* **2014**, *195*, 189–196. [CrossRef]
31. Zhang, W.H.; Zhang, W.D. Fabrication of SnO2−ZnO Nanocomposite Sensor for Selective Sensing of Trimethylamineand the Freshness of Fishes. *Sens. Actuators B Chem.* **2008**, *134*, 403–408. [CrossRef]
32. Chu, X.; Zhou, S.; Zhang, W.; Shui, H. Trimethylamine sensing properties of nano-$LaFeO_3$ prepared using solid-state reaction in the presence of PEG400. *Mater. Sci. Eng. B* **2009**, *164*, 65–69. [CrossRef]
33. Dao, D.V.; Shibuya, K.; Bui, T.T.; Sugiyama, S. Micromachined NH_3 gas sensor with ppb-level sensitivity based on WO_3 nanoparticles thin film. *Procedia Eng.* **2011**, *25*, 1149–1152. [CrossRef]
34. Arienzo, M.D.; Armelao, L.; Mari, C.M.; Polizzi, S.; Ruffo, R.; Scotti, R.; Morazzoni, F. Macroporous WO_3 thin films active in NH_3 sensing: Role of the hosted Cr isolated centers and Pt nanoclusters. *J. Am. Chem. Soc.* **2011**, *133*, 5296–5304. [CrossRef] [PubMed]
35. Srivastava, V.; Jain, K. Highly sensitive NH_3 sensor using Pt catalyzed silica coating over WO_3 thick films. *Sens. Actuators B Chem.* **2008**, *133*, 46–52. [CrossRef]
36. Maekawa, T.; Tamaki, J.; Miura, N.; Yamazoe, N. Gold-loaded tungsten oxide sensor for detection of ammonia in air. *Chem. Lett.* **1992**, *4*, 639–642. [CrossRef]
37. Late, D.J.; Doneux, T.; Bougouma, M. Single-layer $MoSe_2$ based NH_3 gas sensor. *Appl. Phys. Lett.* **2014**, *105*, 233103. [CrossRef]
38. Wu, H.; Ma, Z.; Lin, Z.; Song, H.; Yan, S.; Shi, Y. High-Sensitive Ammonia Sensors Based on Tin Monoxide Nanoshells. *Nanomaterials* **2019**, *9*, 388. [CrossRef]
39. Rout, C.R.; Hegde, M.; Govindaraj, A.; Rao, C.N.R. Ammonia sensors based on metal oxide nanostructures. *Nanotechnology* **2007**, *18*, 205504. [CrossRef]
40. Nguyen, L.Q.; Phan, P.Q.; Duong, H.N.; Nguyen, C.D.; Nguyen, L.H. Enhancement of NH_3 gas sensitivity at room temperature by carbon nanotube-based sensor coated with Co nanoparticles. *Sensors* **2013**, *13*, 1754–1762. [CrossRef] [PubMed]
41. Wang, Y.; Zhang, L.; Hu, N.; Wang, Y.; Zhang, Y.; Zhou, Z.; Liu, Y.; Shen, S.; Peng, C. Ammonia gas sensors based on chemically reduced graphene oxide sheets self-assembled on Au electrodes. *Nanoscale Res. Lett.* **2014**, *9*, 251. [CrossRef] [PubMed]
42. Chen, L.; Tsang, S.C. Ag doped WO_3-based powder sensor for the detection of NO gas in air. *Sens. Actuators B Chem.* **2003**, *89*, 68–75. [CrossRef]
43. Penza, M.; Martucci, C.; Cassano, G. NOx gas sensing characteristics of WO_3 thin films activated by noble metals (Pd, Pt, Au) layers. *Sens. Actuators B Chem.* **1998**, *50*, 52–59. [CrossRef]
44. Wang, S.H.; Shen, C.Y.; Su, J.M.; Chang, S.W. A room temperature nitric oxide gas sensor based on a copper-ion-doped polyaniline/tungsten oxide nanocomposite. *Sensors* **2015**, *15*, 7084–7095. [CrossRef]
45. Ho, K.C.; Tsou, Y.H. Chemiresistor-type NO gas sensor based on nickel phthalocyanine thin films. *Sens. Actuators B Chem.* **2001**, *77*, 253–259. [CrossRef]
46. Tamaki, J.; Hashihin, T.; Uno, Y.; Da, D.V.; Sugiyama, S. Ultrahigh-sensitive WO_3 nanosensor with interdigitated Au nano-electrode for NO_2 detection. *Sens. Actuators B Chem.* **2008**, *132*, 234–238. [CrossRef]

47. Zhang, C.; Debliquy, M.; Boudiba, A.; Liao, H.; Coddet, C. Sensing properties of atmospheric plasma-sprayed WO_3 coating for sub-ppm NO_2 detection. *Sens. Actuators B Chem.* **2010**, *144*, 280–288. [CrossRef]
48. Xia, H.; Wang, Y.; Kong, F.; Wang, S.; Zhu, B.; Guo, X.; Zhang, J.; Wang, Y.; Wu, S. Au-doped WO_3-based sensor for NO_2 detection at low operating temperature. *Sens. Actuators B Chem.* **2008**, *134*, 133–139. [CrossRef]
49. Fruhberger, B.; Stirling, N.; Grillo, F.G.; Ma, S.; Ruthven, D.; Lad, R.J.; Frederick, B.G. Detection and quantification of nitric oxide in human breath using a semiconducting oxide based chemiresistive microsensor. *Sens. Actuators B Chem.* **2001**, *76*, 226–234. [CrossRef]
50. Pan, X.; Zhao, X.; Bermak, A.A.; Fan, Z. A humidity-insensitive NO_2 gas sensor with high selectivity. *IEEE Electron Device Lett.* **2016**, *37*, 92–95. [CrossRef]
51. Maeng, S.; Kim, S.W.; Lee, D.H.; Moon, S.E.; Kim, K.C.; Maiti, A. SnO_2 nanoslab as NO_2 sensor: Identification of the NO_2 sensing mechanism on a SnO_2 surface. *ACS Appl. Mater. Interfaces* **2014**, *6*, 357–363. [CrossRef] [PubMed]
52. Novikov, S.; Lebedeva, N.; Satrapinski, A. Ultrasensitive NO_2 gas sensor based on epitaxial graphene. *J. Sens.* **2015**, *2015*, 108581. [CrossRef]
53. Kneer, J.; Wöllenstein, J.; Palzer, S. Manipulating the gas–surface interaction between copper(II) oxide and mono-nitrogen oxides using temperature. *Sens. Actuators B Chem.* **2016**, *229*, 57–62. [CrossRef]
54. Yoo, R.; Li, D.; Rim, H.J.; Cho, S.; Lee, H.-S.; Lee, W. High sensitivity in Al-doped ZnO nanoparticles for detection of acetaldehyde. *Sens. Actuators B Chem.* **2018**, *266*, 883–888. [CrossRef]
55. Koo, A.; Yoo, R.; Woo, S.P.; Lee, H.-S.; Lee, W. Enhanced acetone-sensing properties of Pt-decorated Al-doped ZnO nanoparticles. *Sens. Actuators B Chem.* **2019**, *280*, 109–119. [CrossRef]
56. Choe, Y.-S. New gas sensing mechanism for SnO_2 thin-film gas sensors fabricated by using dual ion beam sputtering. *Sens. Actuators B Chem.* **2001**, *77*, 200–208. [CrossRef]
57. Cho, H.; Oh, I.; Kang, J.; Park, S.; Ku, B.; Park, M.; Kwak, S.; Khanra, P.; Lee, J.H.; Kim, M.J. Catalyst and doping methods for arc graphene. *Nanotechnology* **2014**, *25*, 445601. [CrossRef]
58. Shimizu, Y.; Matsunaga, N.; Hyodo, T.; Egashira, M. Improvement of SO2 sensing properties of WO3 by noble metal loading. *Sens. Actuators B Chem.* **2001**, *77*, 35–40. [CrossRef]
59. Itoh, T.; Nakashima, T.; Akamatsu, T.; Izu, N.; Shin, W. Nonanal gas sensing properties of platinum, palladium, and gold-loaded tin oxide VOCs sensors. *Sens. Actuators B Chem.* **2013**, *187*, 135–141. [CrossRef]
60. Joshi, R.K.; Gomez, H.; Alvi, F.; Kumar, A. Graphene films and ribbons for sensing of O2, and 100 ppm of CO and NO2 in practical conditions. *J. Phys. Chem. C* **2010**, *114*, 6610–6613. [CrossRef]
61. Lu, Y.F.; Lo, S.T.; Lin, J.C.; Zhang, W.; Lu, J.Y.; Liu, F.H.; Tseng, C.M.; Lee, Y.H.; Liang, C.T.; Li, L.J. Nitrogen-doped graphene sheets grown by chemical vapor deposition: Synthesis and influence of nitrogen impurities on carrier transport. *ACS Nano* **2013**, *7*, 6522–6532. [CrossRef] [PubMed]
62. Usachov, D.; Vilkov, O.; Grüneis, A.; Haberer, D.; Fedorov, A.; Adamchuk, V.K.; Preobrajenski, A.B.; Dudin, P.; Barinov, A.; Oehzelt, M.; et al. Nitrogen-doped graphene: Efficient growth, structure, and electronic properties. *Nano Lett.* **2011**, *11*, 5401–5407. [CrossRef] [PubMed]
63. Shaik, M.; Rao, V.K.; Gupta, M.; Murthy, K.S.R.C.; Jainc, R. Chemiresistive gas sensor for the sensitive detection of nitrogen dioxide based on nitrogen doped graphene nanosheets. *RSC Adv.* **2016**, *6*, 1527–1534. [CrossRef]
64. Dai, J.; Yuan, J.; Giannozzi, P. Gas adsorption on graphene doped with B, N, Al, and S: A theoretical study. *Appl. Phys. Lett.* **2009**, *95*, 232105. [CrossRef]
65. Jappor, H.R.; Khudair, S.A.M. Electronic properties of adsorption of CO, CO_2, NH_3, NO, NO_2 and SO_2 on nitrogen doped graphene for gas sensor applications. *Sens. Lett.* **2017**, *15*, 432–439. [CrossRef]